Nuclear Instruments and Methods in Physics Research B 499 (2021) 133–141

Contents lists available at ScienceDirect

Nuclear Inst. and Methods in Physics Research, B

journal homepage: www.elsevier.com/locate/nimb

Bunching and chopping for tandem accelerators. Part I: Bunching

Nikolai R. Lobanov *, Peter Linardakis, Daniel Tempra

The Department of Nuclear Physics, Research School of Physics and Engineering, The Australian National University, Canberra, ACT 2601, Australia

ARTICLE INFO

Keywords:
Tandem accelerator
Beam bunching
Longitudinal phase space

ABSTRACT

A pulsed system capable of delivering up to a few microamps with a mass range 1–100 u, and with pulse width of bursts of ions approximately 1–2 ns is described. Critical design limitations are discussed to show the overall approach to meet a number of experimental requirements. The system consists of a SNICS negative ion source, a low energy buncher which uses the entire tandem electrostatic accelerator as a drift path to produce bunched ion bursts at the targets or linac entry, and high energy choppers. The buncher consists of a single acceleration gap with aligned removable grids. A detailed analysis is presented of the factors limiting the system performance, with the aim to lessen their effect on the ultimate minimum longitudinal phase space of the ion burst.

1. Introduction

The importance of sub-nanosecond pulsing systems is driven by the demand of time- of-flight techniques in heavy ion experiments and the installation of RF boosters. A typical operational frequency of a booster is 80–160 MHz. In order to achieve the required energy resolution, it is desirable to produce a pulse width at the injection point of the linac as narrow as 50 ps. The ion beam will pass through one or two electron strippers and therefore only a few percent of ions reach the linac. Due to loading limitations of the tandem and the desire for maximum efficiency, the system should be able to bunch a large fraction, i.e. ~ 50%–70%, of the dc beam.

As a first approximation, bunching is a linear operation conserving the longitudinal phase space $\varepsilon_z = \Delta t\, \Delta W$, where Δt is the time spread and ΔW is the energy spread. Analyses and guides for design were reported previously in [1,2]. The nonlinear effects are large enough to prevent pulse widths in the 50–500 ps range to be produced in a one stage system. Therefore, bunching systems consist of a low energy and a high energy buncher separated by accelerator sections including one or two strippers and often followed by a stripper at the entrance of the booster.

A system developed at Argonne [1] employs a harmonic buncher with a single gap carrying an RF sine wave and its higher harmonics. In order to excite the grids with modest power, high Q resonant circuits are employed. Similar systems utilizing 3 and 4 harmonics have been developed at Heidelberg [3], Florida State University [4], New Delhi [5], Michigan State University [6] and Legnaro National Laboratory. Only two higher harmonics are applied at Garching [2] and Saclay [7]. Usually the waveform is applied to the gap by a pair of grids that define the gap boundary and improve the accelerating field homogeneity inside the gap. The grids are non-retractable and consequently always exposed to beams whether they are used for bunching or not. In most cases the grids are made by photo etching 0.005″ thick molybdenum. A long-life grid for heavy ion bunching made of tungsten wire is described in [8]. The use of two grids reduces beam transmission to about 80%, which is unacceptable when accelerating secondary radioactive beams or for AMS applications. In response, Argonne has developed a grid-less multi-harmonic buncher [9]. The main concern in a grid-less bunching system is the uniformity of the longitudinal E-field over the radial coordinate which requires a small beam size at the buncher. Computer calculations and experimental measurements demonstrated no noticeable effect of beam size on the bunching quality. A similar grid-less low-energy pre-buncher system was developed at TRIUMF in Vancouver [10].

Another type of pulsing system is based on a klystron buncher, which is a two gap RF resonator with the optimum distance between the gaps matching the velocity of the ions [11]. This limits its efficient operation to a relatively narrow range of ion beam velocities. In order to overcome this limitation, a versatile system for heavy ions has been developed at the Wetzmann Institute of Science [12]. The buncher is split into four gaps so that by connecting the proper combination of sections to the RF source, one may obtain a two-gap device with drift lengths covering the mass range of ions from 12 to 58.

A ‘double drift’ buncher has been developed at Oak Ridge [13,14] and is utilized in Munich [15] and Stony Brook [16]. The Munich ‘double drift’ buncher consists of two double gap klystron bunchers with variable frequency at ~ 5 and 10 MHz [15]. More general concepts of

* Corresponding author.
E-mail address: Nikolai.Lobanov@anu.edu.au (N.R. Lobanov).

https://doi.org/10.1016/j.nimb.2021.02.013
Received 12 May 2020; Received in revised form 16 September 2020; Accepted 2 February 2021
Available online 6 May 2021
0168-583X/Crown Copyright © 2021 Published by Elsevier B.V. All rights reserved.

multiple bunching cavities operating at higher harmonics of the fundamental frequency with arbitrary spacing have been reported on in [2,17]. An unusual triple harmonic pulsing system has been developed at Legnaro which incorporates features of double-drift, klystron and single gap bunchers [18]. The system is designed for bunching the dc beam produced by the ECR source and accelerated by the PIAVE high voltage platform. Since the ECR source produces higher charge states for heavier ions, the beam velocity and buncher efficiency are independent of atomic mass number M.

All of the bunching systems discussed in the previous paragraphs are based on resonant lines that have to be tuned according to the operational frequency with precise control of the phases and amplitudes of all harmonics. This is an efficient method to generate a few kilovolts of modulation voltage, but it is restricted to rather high frequencies and narrow bandwidths. Amplification using a wide band amplifier of a linear voltage produced at low RF power level has been developed at Lanzhou and Vancouver [19,20]. Because of the high cost of amplification of the low level RF waveform, a high power half-cosine wave generation method has been developed at Texas [21]. This technique takes advantage of the high current and fast switching capability of MOSFETs without the demand for wide bandwidth linear gain. The direct production of a linear waveform at the required voltage by charging a capacitance representing the bunching gap has been proposed at Lanzhou [22] and adopted at Orsay [23]. So far the direct production techniques of sawtooth waveforms are limited up to 1 kV peak voltages on parallel plates, which is required for cyclotron injection beam transport lines. Unfortunately, this voltage is not high enough for injection systems of electrostatic accelerators when bunching light ions.

The various considerations involved in the design of bunching and RF systems take into account buncher waveforms, transit time effects, acceleration field inhomogeneity, grids, optimum frequency and distances. These are analyzed in [1]. Results of a theoretical study of the dynamic focusing effects and energy modulation imperfections of ungridded klystron bunchers are presented in [14]. A simple formalism to analyze a tandem bunching system is presented in [2]. Various factors limiting the performance of the bunching system are summarized in [1,2,17] with the aim of minimizing their inevitable influence on the minimum longitudinal phase space. The ion optical properties of the post-buncher transport system consisting of quadrupole lenses and analyzing magnet and their influence on the time spread of pulsed beam are studied in [24].

The system described in this paper consists of the following components: (1) a low energy room temperature buncher that produces 1 ns pulses at 9.375 MHz frequency; (2) two high energy beam choppers operating at 37.5 MHz and 4.6875 MHz respectively that remove the minor background ions between pulses; (3) an ion burst phase detector that provides the feedback correction signal and; (4) a superconducting resonator at 150 MHz that compresses 1 ns pulses down to 50 ps width. The whole system has been implemented and operated successfully over the last decade. Due to the complexity of the subject, the buncher and operational results are discussed in this paper. The results on high energy choppers will be published in a separate paper. The phase detector, superconducting high energy buncher and a comprehensive operational report will be the subject of a future publication.

The bunching system under consideration is a conventional system with similar characteristics reported in earlier works. In this paper, however, the focus is on theoretical and experimental tools to evaluate performance limitations over a wide range of ion masses and energies. The theoretical treatment in this paper also includes the effects of spherical and chromatic aberration - something that was not considered before in similar systems. Both theoretical and experimental approaches developed in this paper are not limited to single gap buncher systems but can be applied for a variety of designs described in introduction.

This paper has been organized into three main sections. In the first section, analytical expressions of the bunching and chopping processes are derived and factors limiting the performance are reviewed. It introduces an experimental procedure for reliable and reproducible measurement of the beam bunching and transmission through the electrostatic accelerator. The second section presents key analytical calculation and experimental verification of the performance of the buncher and RF control system and beam test results based on selected beam bunching runs at nominal and reduced terminal voltages. The records have been systematically collected during R&D work on the 14UD electrostatic tandem over the last few years. The third section presents interpretation of theoretical and experimental results and relates them to the performance of the pulsing system.

2. Methods

2.1. The generalized concept of bunching and overall system layout

A schematic diagram of the bunching and chopping systems of the tandem accelerator, presenting; the principal components, voltage and beam energy distributions and drift lengths is shown in Fig. 1. The negative ion beam of atomic mass M and single charge state q^- is produced from a modified Source of Negative Ions by Caesium Sputtering (SNICS) [25]. The main low energy components are a decelerating Einzel lens, followed by an immersion lens at ~ 13 kV; an accelerating tube, up to 150 kV; a remotely adjustable object 4-jaw slits; an 82.9 cm radius double focusing 90° dipole bending magnet and adjustable image slits. The specifications of the sector bending magnet are; mass energy product 50 u × MeV/Z^2, object slit distance 2633 mm, image slit distance 2433 mm and momentum dispersion 33 mm/%. The negative ions of energy up to $E_1 = E_{inj} = 0.155$ MeV enter a multi-harmonic single gap buncher to which combined sine waves are applied of frequencies 9.375 MHz, 18.75 MHz and 28.125 MHz.

A detailed description of the bunching system and associated electronics is presented in reference [26], which outlines the general concept of the mechanical design of the buncher with retractable grids and describes a novel concept of the RF control system. The bunched beam becomes substantially compressed into ion bursts during passage through the low energy drift space of length S_1 and enters a low energy accelerating tube spanning distance S_2 comprising 6 units of the 14UD tandem. The beam exits this section of the accelerator gaining a total energy $E_{2[MeV]} = E_{inj} + 6q^-U_T/14$, where U_T is the voltage applied to the terminal in MV. Subsequently the beam passes through a field free low energy middle section of length S_3 with no energy gain $E_3 = E_2$. This is followed by further acceleration in the second section of low energy acceleration tube with the length S_4 to the final energy $E_4 = E_{inj} + q^-U_T$. Then, negative ions arrive and travel through the terminal of length S_5 without acceleration, $E_5 = E_4$. In the terminal they pass through either a gas channel or a thin carbon foil that strips electrons from the ions, resulting in positively charged ions of charge state Q_1, which enter the high energy section S_6 of the tandem accelerator which comprises $4^2/_3$ units. The ions exit this section at the final energy $E_6 = E_{inj} + q^-U_T + 4^2/_3Q_1U_T/13^2/_3$, since the total number of units in the high energy branch of 14UD accelerator is $13^2/_3$. At this point ions pass through the last field free region, called the high energy middle section, of length S_7 without energy gain, $E_7 = E_6$. In this section the heavy ions have enough energy for efficient second stripping to charge state Q_2 by passing through another stripping carbon foil. Finally ions pass through the final high energy column, S_8, of the tandem comprising 9 units, gaining the maximum energy $E_{out} = E_8 = E_{inj} + q^-U_T + 4^2/_3Q_1U_T/13^2/_3 + 9Q_2U_T/13^2/_3$. Typically, the high energy beam stability is better than ± 2 keV multiplied by the accelerated ion charge. The bunched bursts of ions are finally focused by a high energy magnetic quadrupole through two pairs of chopper deflector plates operating at 4.6875 MHz and 37.5 MHZ and a 4 jaw object slit unit at a distance of S_9 from the end of the accelerator followed by a mass-energy product $ME/Q^2 = 200$, 1.27 m radius double focusing 90° energy analyzing magnet and 2 jaw image slits.

Chopper 1 at 37.5 MHz cuts off the tails of the bunched beam by providing a time window of ~ 2 ns every 13.3 ns and sweeps the beam in

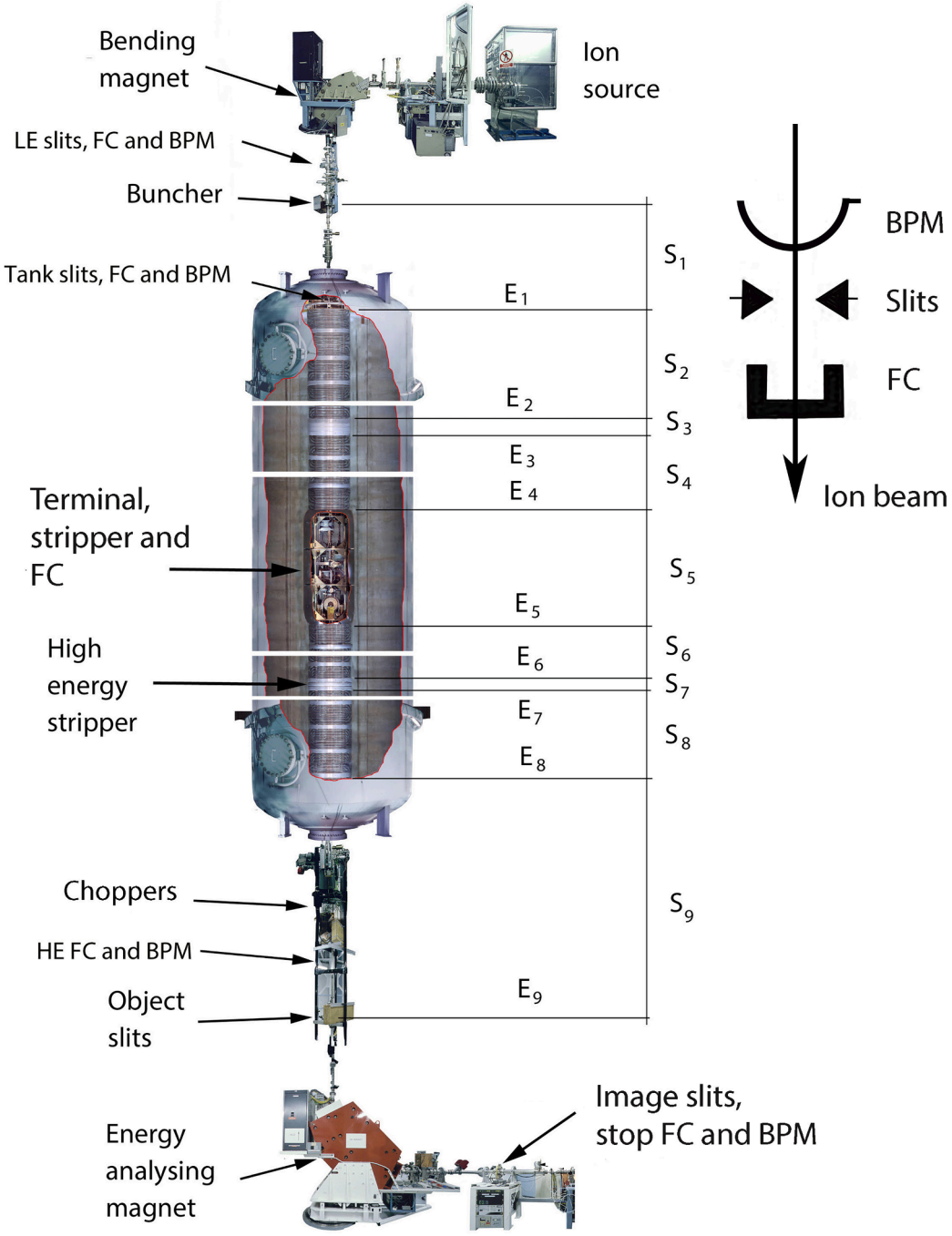


Fig. 1. Bunching and chopping systems for a tandem accelerator. The accelerator structure is simplified by separating it into different segments of length S and of two types of sections: drift ($S_1 = 3.3$ m, $S_3 = 0.3$ m, $S_5 = 3$ m, $S_7 = 0.19$ m and $S_9 = 12.48$ m) and accelerating sections ($S_2 = 3.48$ m, $S_4 = 4.64$ m, $S_6 = 2.71$ m and $S_8 = 5.22$ m). The low energy (LE), tank (T), high energy (HE) and stop (S) beam profile monitors (BPM) and Faraday cups (FC) are used to determine transmission through the machine. The inset shows the typical combination of BPM, slits and FC.

the non– dispersive plane of the energy analyzing magnet which corresponds to the X direction at the defining aperture. Since the buncher has a repetition interval of 106.7 ns, the satellite low intensity pulses are eliminated by Chopper 2 operating at 4.6875 MHz and providing a 6 ns window every 106.7 ns centered on the desired Chopper 1 window that is populated by the buncher. Chopper 2 deflects the beam in an energy dispersive plane which translates to the Y direction at the aperture. The distance from Chopper 1 and Chopper 2 to the object slits is 3.07 and 2.83 m respectively. The distance between the choppers is 0.24 m. The beam can be directed into either of two target areas or into the LINAC booster for further acceleration. The beam injected into the LINAC has been compressed to a width as little as one nanosecond and then is further compressed to a width of ~ 100 ps by the superconducting buncher made up of a $\beta = 0.1$, quarter-wave resonator.

It is shown [27] that for bunching calculations, the successive lengths of drift spaces and accelerating sections through which beam passes can be replaced by a single equivalent drift length. In the case of the tandem accelerator, the predominant dimension is the low energy drift length S1 and the first section of the accelerating column S_2. The remaining accelerating tubes contribute only a small proportion of the effective drift length. Thus Fig. 1 can be replaced by the simplified system in which Ś represents the low energy equivalent effective drift

length between the buncher gap and the target. Reduction of the system to the simple form enables the calculation of bunched current waveforms at the target.

It can be shown [15] that bunching occurs and a waveform with a single infinitely narrow peak is obtained when

$$\pi\xi f_b S/v = 1 \tag{1}$$

where ξ is the ratio of the peak sine wave modulation energy ΔE_m to the mean ion energy E, $f_b = 9.375$ MHz is the frequency of bunching voltage applied to the gap, S is the drift distance over which the beam of velocity v becomes compressed. In real bunching systems the pulse length at the target is fundamentally limited by the beam longitudinal emittance. As a first approximation, the velocity of an ion with atomic mass number M and energy $E_{[MeV]}$ is given by the expression

$$v = c(2E/931.5M)^{1/2} = 0.046c(E/M)^{1/2}, \tag{2}$$

where c is the speed of light in vacuum and 931.5 MeV/c^2 is the rest mass of atomic mass unit. Substituting (2) into (1) one now arrives at the equation for the drift distance S

$$S_{[m]} = \left(0.046c/\pi f M^{1/2}\right)E^{3/2}/\Delta Em \tag{3}$$

It follows from Eq. (3) that the equivalent drift length of any field free region identified with index 'i' is given by equation

$$S'_i = S_i(E_1/E_i)^{3/2} \tag{4}$$

where $E_1 = E_{inj}$ is the mean energy of ions in the low energy drift space where the modulation energy is applied. In case of i = 1, the equation (4) is simplified to $\dot{S} = S_1$. Dividing (4) by (2) and assuming E = E_1, one now arrives at the equation for the equivalent transit time of any field free region

$$T'_i = S_i M^{1/2} E_1 E_i^{-3/2} \Big/ 0.046c, \tag{5}$$

The equivalent drift length of the region 'i' with a constant gradient acceleration field is calculated [26] by the expression

$$S'_i = 2S_i(E_1/E_i)\left((E_1/E_{i-1})^{1/2} - (E_1/E_i)^{1/2}\right) \tag{6}$$

where indexes; 'i-1′ and 'i' refer to the entrance and exit of the acceleration stage respectively. The equation for the equivalent transit time for a region with a constant gradient acceleration field becomes

$$T'_i = 2S_i(E_1 M)^{1/2}((E_1/E_{i-1})^{1/2} - -(E_1/E_i)^{1/2})/(0.046cE_i) \tag{7}$$

It should be noted that equations (4) to (7) are valid for values Em«E_1, and $E_m = 0.1E_1$ should be taken as a maximum value.

2.2. Effects of energy spread on beam pulse broadening and overall transmission

An energy spread introduced into the ion beam at any point in the system will result in a time spread and loss of amplitude of a bunched pulse at the target. Here we discuss the effects of random energy variations. The effects of synchronous energy spread are not considered on the assumption that the phase detection feedback loop corrects for these things. Another cause of transit time variation is the path length variation through the ion beam optics elements such as; the Einzel lens, the quadrupole lens and the dipole magnet. In addition, loss of beam intensity at the target is caused by chromatic aberration of the optical components due to the energy spreads introduced by the bunching or stripping systems.

2.2.1. De-bunching due to ion energy spread

In the case of the bunching system, if ΔE_1 is the energy spread existing in the ion beam before energy modulation is applied by the buncher, then the resulting time spread Δt_1 at the target is given [1] by

$$\Delta t_1 = 1/2\Delta E_1 S'(E_1 v)^{-1}, \tag{8}$$

where S' = ΣS_i is the effective drift length from the buncher to the target. Substituting (2) into (8) one now arrives at the practical equation for time spread

$$\Delta t_1 = 1/2S' M^{1/2}(\Delta E_1/E^{3/2})/0.046c \tag{9}$$

where Δt_1 is in s, ΔE_1 and E_1 are in MeV. The energy spread of the Middleton-type ion source was measured in [28]. It was reported that the spectrum depended on operating conditions of the source, but typically the full width at half-maximum was of the order of ~ 10–12 eV for $^{12}C^-$, $^{32}S^-$ and $^{122}I^-$ ions. The energy spectrum of the ion beam extracted from a SNICS source was reported in [29]. The peak of the spectrum occurred at 5–16 eV and the FWHM was in the range of about 23–38 eV. For the energy spread of the ion source we assume the value $\Delta E_1 = 40$ eV.

In the case of the stripping system, the transit time difference, Δt_s, at the output of the tandem accelerator is caused by the energy spread ΔE_s induced by terminal stripping. It can be calculated from Eq. (9) by substituting corresponding values

$$\Delta t_{s[s]} = 1/2S'_s M^{1/2}(\Delta E_s/E^{3/2})/0.046c, \tag{10}$$

where E_s is the energy of the beam arriving at the stripper and $\dot{S}_s$ is the effective drift length from stripper to target. The stripper energy spread ΔE_s consists of two components: energy loss straggling and carbon foil inhomogeneity. According to data presented in [2], the typical stripper induced energy spread for 13 MeV ions and 5 μg/cm^2 carbon foil can be approximated by linear dependence $\Delta E_s = 0.6$ M for a projectile mass number M in the range from 1 to ~ 50 and a constant value of ~ 30 keV for M > 50. Therefore, the transit time spread induced by the stripper is increasingly important for heavy ions.

2.2.2. Beam path length variation

The angular spread of the beam causes deviations in path length. Consider particles travelling at angle θ in relation to the straight beam axis. The transit time changes as $\Delta t/t = \Delta L/L \approx \frac{1}{2}\theta^2$ [1]. The effective time spread due to path differences from the source to the target is given by the equation

$$\Delta t\theta \approx 1/2\Sigma\theta_i^2 T'_i \tag{11}$$

where T'_i is calculated from equation (7) and θ_i is a convergence or divergence angle corresponding to drift length "i". In the case of the Pelletron accelerator, the major contributors to transit time is the low energy drift length S_1 and the first section of accelerating column S_2, the remaining sections add only a small fraction of the transit time broadening. The typical value of θ in the low energy section of the accelerator is ~ 10 mrad.

In a conventional 90° double-focusing energy analyzing magnet the time spread due to path length differences are of the order of

$$\Delta t_\alpha \approx 4\alpha\rho/v, \tag{12}$$

where ρ is the radius of curvature and $\alpha \approx 2.5$ mrad is the angle between particles and axis in the crossovers at external object and image locations and v is the velocity of ions calculated by the formula (2) [1,30].

2.2.3. Loss of transmission due to spherical and chromatic aberrations of the ion optics

Each particle at the electrostatic accelerator entrance is described by six independent degrees of freedom. In a Cartesian coordinate system they are the horizontal and vertical coordinates and their related momenta x , p_x, y, p_y and the energy and phase relative to a reference particle w, ϕ. Thus, a beam is fully described by the distribution of particles in the 6D phase space. The two dimensional projections ε_x, ε_y and ε_z of 6D distribution are called emittances [30]. If degrees of

freedom are not correlated, the uncorrelated 6D distribution is calculated by the formula $\varepsilon_6 = \varepsilon_x\varepsilon_y\varepsilon_z$. A typical normalized 2D emittance of a SNICS ion source for 90% of the beam is up to $\varepsilon_n = \varepsilon\beta\gamma \sim 9\ \pi$ mm mrad MeV^{½} [29,31]. The acceptance of the electrostatic accelerator has the dimension of emittance and thus must be greater to ensure lossless beam transmission through the system. There are a variety of effects that can lead to the emittance growth of a particle beam: scattering in a foil, interactions with residual gas, power supply ripple and spherical and chromatic aberrations of optical components. One measure of aberrations is given by the radius of the disk of least confusion, r, which represents the Gaussian image plane and defines the smallest spot formed by the lens system. The radius, r_s, due to spherical aberration is related to the angular convergence of the beam, θ, in the drift space $r_s = C_s\theta^3$, where C_s is the coefficient of spherical aberration [32]. For a weak lens $C_s \approx f$, where f is the focal length of the lens. For the strong lens, C_s falls below f. In the accelerator systems under investigation, typical values are $C_s \approx f \approx 1500$ mm and $\theta \approx 10$ mrad resulting in $r_s < 0.002$ mm. Therefore the effect of spherical aberration on pulse widening and reduction of transmission can be neglected.

The bunching length increases linearly with a reduction in the bunching voltage, but increases with the 3/2 power of the particle energy. So, to attain a short flight path, it is essential to bunch a low energy beam E_1 with high-voltage modulation ΔE_m. This is just the situation that will reduce the transmission in the low energy ion optical system due to chromatic aberration. When ions are present with energy E and a half value of total energy spread ΔE, they will be focused at different distances from a lens and there will be a chromatic disk of confusion with radius r_c rather than a point focus [32]. A coefficient of chromatic aberration C_c is defined by the equation

$$r_c \approx \theta C_c(\Delta E/E), \tag{13}$$

where θ is the angular convergence of the beam. Typically $C_c = f$ in the thin lens approximation. A thick lens treatment gives a slightly smaller C_c for a weak lens and f/2 for a strong lens. In the case of the Pelletron, the major contributor to r_c is the low energy section of the accelerating column, since in the remaining high energy sections the ratio ΔE/E becomes very small. The typical value of θ in the low energy section of accelerator is ~ 10 mrad and $C_c \approx f \approx 1500$ mm.

2.2.4. Loss of transmission due to non-achromatic properties of energy analyzing magnet

In orthodox 90° double-focusing energy analyzing magnets, the energy dispersion ΔE causes beam position displacement in the vertical direction Y_{slits} at the two-jaw image slits according to low angle approximation expression [33]

$$\Delta Y_{slits} = 1/2(\rho + D_i)\Delta E/E, \tag{14}$$

where $\rho = 1270$ mm is the bending radius, $D_i = 3\rho$ is the image distance in the vertical plane and E is the beam energy. The beam displacement in the magnet depends on the energy and therefore causes beam cross-section broadening at the slit position. It should be noted that partial loss of transmission is expected if $\Delta Y_{slits} > 0.2a_0$=, where $2a_0$ is the gap between slits.

2.3. Experimental procedures for measurement of the performance of bunching and chopping systems

The experimental conditions are similar to those described in [34]. For typical operational conditions the maximum beam intensity at the HE end of the accelerator was limited to ~ 1 μA and therefore space-charge effects on transmission and time focus formation are negligible. The main beam diagnostic components are a combination of beam profile monitors (BPM), electrically suppressed Faraday cups (FC) and bunch length measurement systems. The beam transport is arranged from waist to waist by choosing the position of the slits. The BPM is always positioned before the slits and the FC is placed after it. This array of BPM and FC allows determination of partial transmission data for any accelerator section confined between two consequent slits. This is important to determine which section of the accelerator is responsible for transmission loss under any given operation conditions. Partial transmission data were obtained for the following sections of the accelerator:

1. The section from the LE slits up to the buncher gap including the LE BPM and the LE FC (Fig. 1). During all transmission tests the low energy and tank slits were set at ± 1.2 mm
2. The injection section of length $S_1 = 3.3$ m which spans from the buncher grids up to the entrance of the acceleration tube with the tank 4-jaw slits, BPM and tank FC (Fig. 1).
3. The LE section of the accelerator from the tank slits up to the terminal. The terminal FC is capable of measuring both negative beam current before electron stripping and positive beam current after stripping
4. The HE section of accelerator from the terminal up to HE object slits. During transmission tests, the HE object slits were set at $2a_0$=±0.9 mm.
5. The beam line from the 90° magnet's object slits to the energy analyzing 2-jaw image slits with stop BPM and stop FC just after the image slits (Fig. 1). The HE image slits were set at $2a_0$=±0.9 mm. The total length of this line is ~ 7.1 m. Exploiting the energy dispersion of the 90° magnet, the vertical Y trace of the stop BPM is used to evaluate the energy spread introduced by the buncher and (or) chopper action according to equation (14) where the rms energy spread due to the combined effect of bunching and stripping is $\Delta E_q = (\Delta E_m{}^2 + \Delta E_s{}^2)^{½}$, where ΔE_m is described in (1) and ΔE_s is discussed in section 2.2.1.
6. The horizontal beam line of length 16.83 m from the image slits toward the superconducting high energy buncher armed with the beam pulse diagnostic system, buncher BPM and FC. The beam pulse monitoring system allows measuring the characteristics of bunches in the time domain. With proper calibration, it is possible to produce an absolute measurement of a pulse's FWHM and relative time of arrival. Therefore the different factors affecting transit time through the accelerator can be experimentally investigated.

The performance criteria of the accelerator are the transmission efficiency and the beam position and size at the high energy image slits. The operation conditions of the BPM used in this work are described in [33]. The minimum resolved beam current with BPM is ~ 0.8nA. The achievable spatial resolution is limited to about 0.5 mm by the diameter of the scanning molybdenum wire. The analysis of the helical wire's quasi-linear motion through the beam leads to a calibration distance given by the expression $d_f = \pi r/\sqrt{2}$, where for the BPM model used, $d_f =$ 6.0 cm is the distance between fiducial marks and r = 2.7 cm is the scanning circle radius. The conversion of the oscilloscope time axis $\Delta T_{osc\ [ms]}$ into a horizontal or vertical displacement of particles is given by the formula $\Delta X_{BPM}[cm] = d_f\Delta T_{osc}/\tau_f$, where $\tau_f = 33$ ms is the time interval between two fiducial signals displayed on an oscilloscope. The oscilloscope time resolution is about 0.2 ms. Therefore the beam displacement resolution measured with the BPM is $\Delta X_{BPM}/d_f = 0.2/33 = 0.6\%$.

The beam pulse diagnostic system is based on γ–ray detection produced by an ion beam striking a tantalum target. The monitoring system measures the time difference between prompt γ–rays and the reference RF synchronizing the entire facility. A comprehensive account of the beam pulse measurement system and its calibration is given in [34]. The pulse width resolution is 0.4 ns. This error is just acceptable to measure the performance of the bunching/chopping systems.

3. Results of analytical calculations and experimental performances of the bunching system

3.1. The results of buncher analytical calculations and performance

The calculated equivalent effective drift length for the entire accelerator, required bunching energy modulation ΔE_m, the rms energy spread due to bunching and stripping $\Delta E_q = (\Delta E_m{}^2 + \Delta E_s{}^2)^{½}$, time spreads at the image slit position Δt_1, Δt_s, Δt_θ, Δt_α, the rms time spread due to combined effect of all above $\Delta t_q = (\Sigma \Delta t_i^2)^{½}$, the radius of the chromatic disk of confusion r_c and the beam position displacement in the vertical direction Y_{slits} at image slits for given values of ion injection energy E1 and terminal voltage U_T are given in Table 1. The rms energy spread is calculated by adding ΔE_m and ΔE_s in quadrature assuming that energy broadening effects are independent. In Table 1 the results are shown for a range of ion atomic masses and three typical sets of operation parameters:{1} high $E_1 = 155$ keV and high $U_T = 14.5$ MeV; {2} low $E_1 = 85$ keV and high $U_T = 14.5$ MeV and {3} high $E_1 = 155$ keV and low $U_T = 3$ MeV.

In Table 1 the numbers in parenthesis refer to equations. The distance from buncher gap to the entrance of accelerating tube is 3.3 m. The total distance from buncher to high energy image slits is 44.2 m much longer than the effective bunching length Ṡ. For the energy spread of the ion source to calculate Δt_1 the value $\Delta E_1 = 40$ eV was assumed.

The experimental LE and HE transmission data are shown in Table 2 as a ratio I_p/I_{dc}, where I_p is the pulsed beam intensity at the optimum bunching field with both choppers turned off and I_{dc} is the dc beam current. The ratio I_p/I_{dc} is a useful parameter to judge the importance of the energy spread introduced by the buncher on beam transmission through LE and HE segments of accelerator. The LE section of 14UD accelerator comprises the segment from the ion source up to the terminal. The HE is the segment starting from stripper position in the terminal and finishing at the stop Faraday cup after the 90° analyzing magnet. The measured pulse width Δt_{exp} (FWHM) is shown at the optimum bunching voltage. The calculated and measured dependencies of transit time Δt_1 and Δt_s on injection E_1 and terminal voltage U_T for several beam parameters are given in Table 2 as ratios $\Delta t_1/\Delta E_1$ and $\Delta t_s/\Delta U_T$.

In Table 2, the beam parameters are shown in a different manner as compared to Table

1. The injection ratio is presented as a ratio of injection voltage E_1 to the terminal voltage U_T. The terminal ratio is the division of the terminal voltage U_T by the 14UD nominal operation voltage $U_n = 14.5$ MV. The transit time measurements have not been accomplished for high energy proton beams (the first line in groups {1} and {2}, Table 2, due to radiation limitations in the accelerator hall accommodating the beam pulse diagnostic system. Furthermore, transit time measurement is not possible for heavy ions at low energy, the last line in group {3}, due to poor sensitivity of the BaF_2 scintillation detector in such operating settings. The overall transmission data from LE to HE can be derived by multiplication of partial transmissions through the LE and HE segments.

Fig. 2 is a consolidated graphical representation of data presented in Tables 1 and 2. Similar to Tables 1 and 2, the graphs are grouped according to three sets of operational parameters according to the injection ratio E_1/U_T. The graphs in the left column of Fig. 2 (a, c and e) compare the performance of the accelerator at high U_T and different injection voltages E_1. The graphs in the right column (Fig. 2 b, d and f) illustrate the performance at constant E_1 and different U_T, including very low terminal voltage (~5 MV).

Fig. 3 presents an example of X and Y half-profiles obtained with the stop BPM at the energy analyzing image slits as described Section 2.1 for a 49 MeV $^7Li^{3+}$ beam.

The single stripped $^7Li^{3+}$ beam energy is 49 MeV and the beam current measured at stop FC is 41nA. The negative $^7Li^{1-}$ ions of energy $E_1 = E_{inj} = 0.105$ MeV are bunched to produce time focus at the beam pulse diagnostic system. The required amplitude of the modulation voltage, calculated with equation (1), is $\Delta E_m = 1.8$ kV. The energy spread introduced by the buncher results in an increase of beam size in the energy dispersive Y direction from 1.99 to 2.16 mm as shown by the grey dots in Fig. 2. The dc beam is shown in black dots. The X profile is not affected by the buncher action remaining at 1.77 mm for dc or bunched beam.

The image depicted in Fig. 4 is a typical plot obtained by the beam pulse monitoring system. The data in this figure are collected by the multichannel analyzer (MCA) connected to the monitoring station just before the superconducting high energy buncher. The beam is 49 MeV $^7Li^{3+}$ produced by the 14UD operating with a single electron stripper at the terminal. The beam is injected at an energy of 69 keV and pulsed with the single frequency low energy buncher.

A Gaussian fit is performed for each peak in order to obtain FWHM and the peak position. The separation between two peaks in Fig. 4 is 106.67 ns corresponding to the bunching frequency of 9.375 MHz. The position of the first and the second peak is 1054 and 2569 channels respectively. Therefore, the calibration factor is 0.0704 ns/channel. The measured FWHM time width of bunched beam is 2.3 ns.

4. Discussion

The calculations and experimental data given in Table 1 and Fig. 2 confirm that the predominant dimension of the effective drift length Ṡ is

Table 1
The calculated equivalent drift length, optimum bunching energy, energy spreads, time spreads and displacements at the image slits for various beam parameters.

Ion	Ṡ m	ΔE_m keV	ΔE_q keV	Δt_1 ns	Δt_s ns	Δt_θ ns	Δt_α ns	Δt_q ns	r_c, mm	ΔY_{slits} mm
{Group}	(4, 6)	(1)		(8)	(10)	(11)	(12)		(13)	(14)
$^1H^{1+}$ {1}	3.47	9.1	9.1	0.08	0.0	0.03	0.34	0.35	0.82	0.79
$_7Li3+$	3.47	3.4	5.4	0.2	0.03	0.08	0.64	0.68	0.31	0.24
$^{16}O^{6+}$	3.46	2.3	9.9	0.3	0.08	0.12	0.73	0.8	0.21	0.25
$^{28}Si^{8+}$	3.46	1.7	16.9	0.4	0.17	0.16	0.85	0.97	0.16	0.33
$^{58}Ni^{12+}$	3.46	1.2	30.0	0.57	0.37	0.23	1.0	1.23	0.11	0.40
$^{107}Ag^{13+}$	3.46	0.9	30.0	0.78	0.5	0.31	1.3	1.63	0.08	0.38
$^1H^{1+}$ {2}	3.39	3.42	3.48	0.20	0.0	0.04	0.34	0.40	0.60	0.30
$^7Li^{3+}$	3.39	1.30	4.40	0.53	0.03	0.11	0.64	0.84	0.23	0.19
$^{16}O^{6+}$	3.39	0.86	9.64	0.79	0.08	0.17	0.73	1.09	0.15	0.24
$^{28}Si^{8+}$	3.39	0.65	16.8	1.1	0.17	0.22	0.85	1.42	0.11	0.33
$^{58}Ni^{12+}$	3.39	0.45	30.0	1.5	0.32	0.23	1.0	1.85	0.08	0.40
$^{107}Ag^{13+}$	3.39	0.33	30.0	2.1	0.43	0.31	1.3	2.53	0.06	0.38
$^1H^{1+}$ {3}	4.04	7.86	7.88	0.09	0.03	0.03	0.74	0.75	0.71	3.2
$^7Li^{3+}$	3.98	3.0	5.16	0.23	0.33	0.09	1.4	1.46	0.27	1.1
$^{16}O^{6+}$	3.95	1.99	9.80	0.34	0.82	0.13	1.6	1.83	0.18	1.2
$^{28}Si^{8+}$	3.95	1.51	16.9	0.45	1.7	0.17	1.9	2.59	0.14	1.6
$^{58}Ni^{12+}$	3.94	1.05	30.0	0.65	3.8	0.24	2.2	4.45	0.1	1.9
$^{107}Ag^{13+}$	3.94	0.77	30.0	0.88	5.3	0.32	2.9	6.11	0.07	1.8

Table 2
The effect of pulsing at optimum bunching electric field amplitude on beam transmission relative to transmission of dc beam and calculated and measured dependencies of transit time on injection and terminal voltage for several beam parameters.

Ion	E_1/U_T%	U_T/U_n	I_p/I_{dc} LE,%	I_p/I_{dc} HE,%	Δt_{exp}, ns	$\Delta t_1/\Delta E_{1calc}$ ns/kV	$\Delta t_1/\Delta E_{1exp}$ ns/kV	$\Delta t_s/\Delta U_{Tcalc}$ ns/kV	$\Delta t_s/\Delta U_{Texp}$ ns/kV
{Group}						eq. (6, 7)		eq. (10)	
$^{1}H^{1+}$ {1}	1.29	0.83	38.8	74.3					
$^{7}Li^{3+}$	1.26	0.85	81.7	90.4	1.4	8.2	9.6	0.03	0.05
$^{16}O^{6+}$	1.27	0.84	97.4	94.8	1.78	7.9	8.2	0.11	0.1
$^{58}Ni^{12+}$	1.29	0.83	99.1	90.8	2.4	15.6	15.7	0.2	0.18
$^{1}H^{1+}$ {2}	0.74	0.83	86.0	98.8					
$^{7}Li^{3+}$	0.69	0.85	90.8	99.7	1.75	17.9	24.3	0.04	0.038
$^{16}O^{6+}$	0.73	0.84	94.9	100.	2.32	18.3	19.2	0.11	0.12
$^{58}Ni^{12+}$	0.74	0.83	98.1	97.9	3.6	35.6	36.2	0.2	0.14
$^{1}H^{1+}$ {3}	3.3	0.29	75.5	53.2	2.1	3.4	4.1	0.05	0.06
$^{7}Li^{3+}$	3.06	0.35	92.6	80.8	2.9	7.8	7.9	0.38	0.36
$^{16}O^{6+}$	3.1	0.34	99.9	97.9	3.7	7.9	7.92	0.4	0.38
$^{58}Ni^{12+}$	3.1	0.34	100.	93.7					

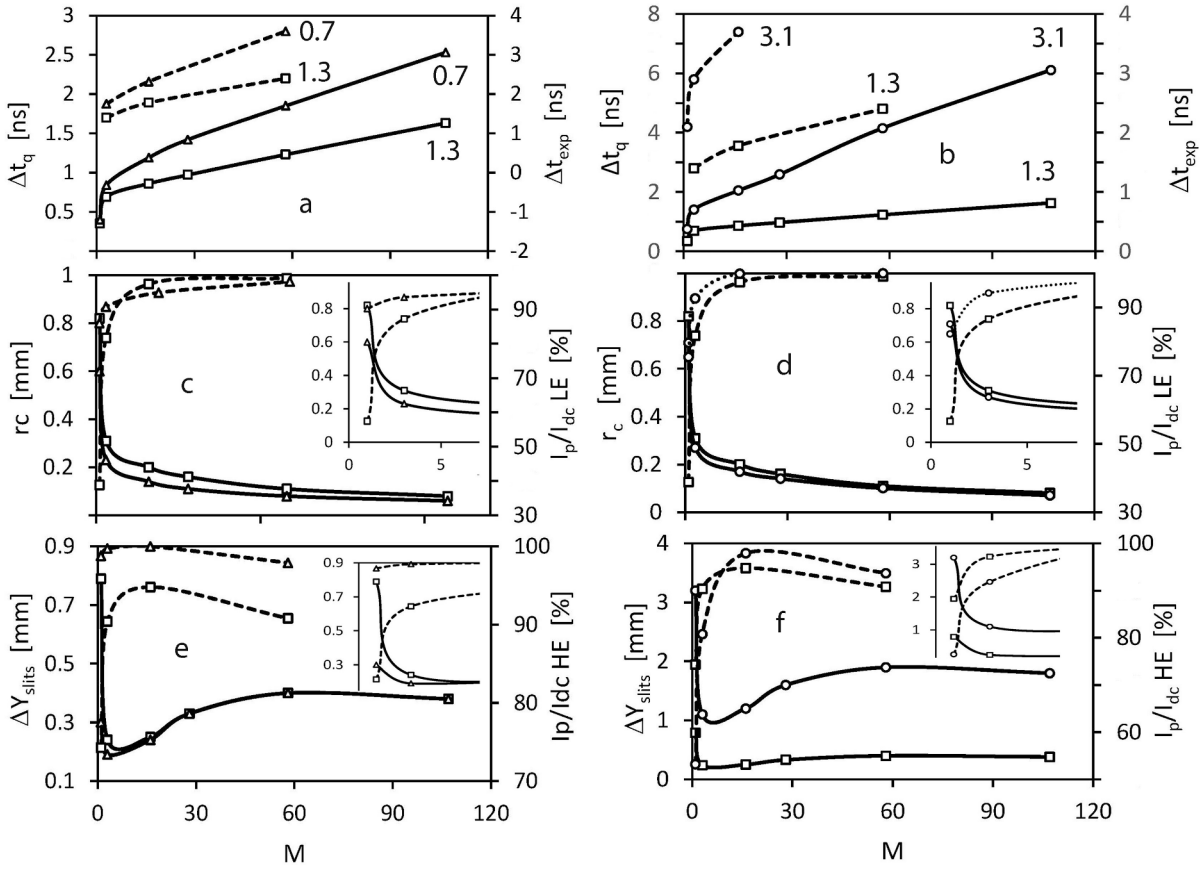


Fig. 2. The calculated data reported in Table 1 and presented as a graph (solid line): the rms combined time spread Δt_q, the radius of a chromatic disk of confusion r_c and the beam displacement in energy dispersion plane of analyzing magnet ΔY_{slits} plotted as a function of M. The experimental data given in Table 2 (broken line): the pulse width at optimum bunching conditions Δt_{exp}, the LE and HE transmission I_p/I_{dc} (LE or HE) as a function of M. The graphs are presented for three main operational parameters of accelerator: {1}- square for which the injection ratio is $E_1/U_T = 1.3$; {2}- triangles, $E_1/U_T = 0.7$; and {3}- circle, $E_1/U_T = 3.1$. The numbers next to graphs show the injection ratio E_1/U_T. The insets show the same graphs zoomed in at low M.

the low energy drift distance $S_1 = 3.3$ m. The remaining accelerating tubes and columns contribute only a small percentage ~ 5% of the effective drift length, required for bunching the ion beam, by applying a modulation voltage ΔE_m. The total time of flight to time focus defines the buncher amplitude, no matter the specific velocity profile during acceleration. It follows from equation (1) that $\Delta E_m/E_1$ is proportional to particle velocity v. Therefore for bunching light particles, higher modulation energy ΔE_m is required. In some cases lowering the injection voltage E_1 is beneficial. The rms energy spread due to the combined effect of bunching and stripping ΔE_q is a V-shape function of atomic mass with a dip at M ~ 10. The rms time spreads at the image slit position due to the combined effects of ion source, stripper and beam path differences, Δt_q, also increases with M, Fig. 2a,b. Therefore it is more difficult to bunch heavy ions into short pulses as compared to light particles, especially at lower injection and, more importantly, reduced terminal voltages, as shown in data sets {2}, Table 1 or Fig. 2a and {3}, Fig. 2b.

Pulsing at the optimum bunching field amplitude may cause deterioration of beam transmission expressed as I_p/I_{dc} in Table 2 and shown as graphs in Fig. 2. The experimental pulse width Δt_{exp} correlates well

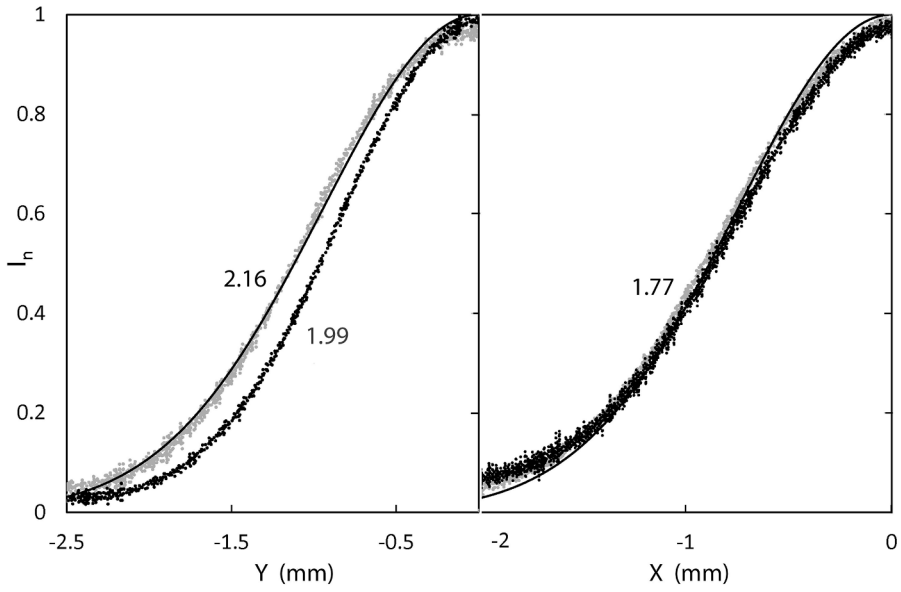


Fig. 3. Normalized half distributions of 49 MeV $^{7}Li^{3+}$ beam horizontal X (right image) and vertical Y (left image) profiles measured with the stop BPM at energy analyzing image slits. The Y direction corresponds to the energy dispersive plane. Profiles produced with a dc beam (black dots) and bunched beam at the optimum bunching RF field (grey dots) with the amplitude ΔE_m = 1.8 kV calculated according to equation (1). The solid line is Gaussian fit of measured profile. The number next to the distribution is the full width of the beam at half its maximum intensity (FWHM) in millimeters.

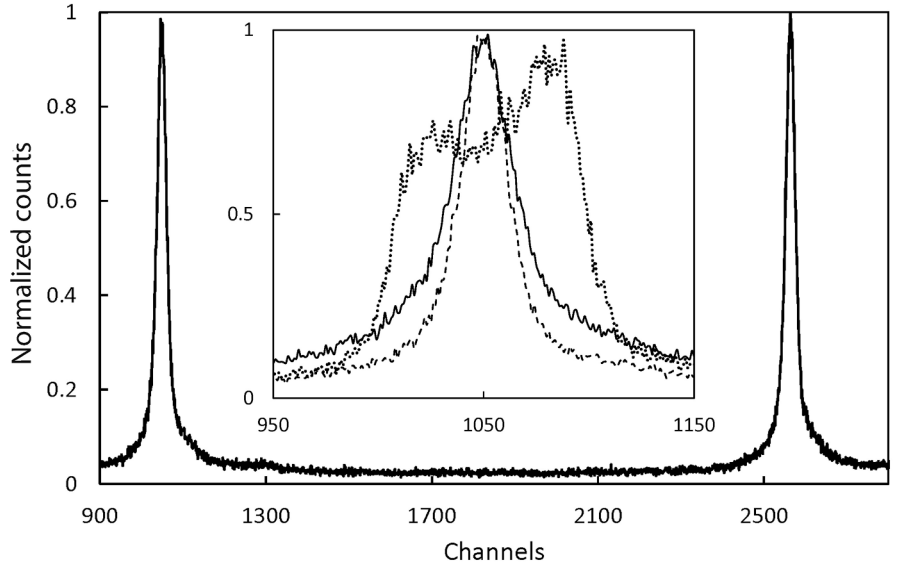


Fig. 4. The histogram shows the beam pulse time profile with the low energy buncher operating at nominal electric field of ΔE_m = 0.95 kV. The collection time for the histogram was 60 s. The time separation between two peaks of 106.67 ns relates to the buncher operation frequency of 9.375 MHz. The inset shows the expanded view of the left peak and the effect of the field modulation ΔE_m on the pulse profile: optimum bunching at ΔE_m = 0.95 kV (dashed line), under-bunching at ΔE_m = 0.86 kV (solid line) and over-bunching at ΔE_m = 1.19 kV (dotted line).

with calculated curve for Δt_q, Fig. 2a,b. In contrast, the transmission graphs have the opposite trend: higher values of r_c and ΔY_{slits} correspond to lower LE or HE transmission, Fig. 2 c,d,e,f. The overall trend for LE and HE experimental transmission data and pulse width Δt_{exp} measurements is very similar to the analytical calculation results, presented in Table 1 and Fig. 2. LE transmission of a beam with energy spread ΔE_m is limited by chromatic aberration of low energy beam transport. Since r_c is directly proportional to ΔE_m, the chromatic aberrations will cause an increase in the radius of chromatic disk of confusion, therefore compromising the overall transmission and this effect is more important for light ions as confirmed by data in set {2} Table 1 or Fig. 2 c,d (inset). To summarize, poor LE transmission is expected for light ions due to chromatic aberrations and the solutions are achromatic optics or a reduction of E_1 and consequently ΔEm.

The HE transmission of beam with energy spread ΔE_q is mainly affected by non-achromatic properties of dipole magnets, according to equation (14), and causing the increase of beam size Y_{slits} at the image slits, Table 1 and Fig. 2 e,f. The Y_{slits} dependence on M has the basic "U" shape, Fig. 2 e,f. For light ions it is dominated by an energy spread introduced by the buncher modulation voltage. The reduction of E_1 and ΔE_m is the effective solution for light ions, Fig. 2e (inset). In case of heavy ions, the energy spread is dominated by the stripper and can be reduced by selecting a stripper foil of minimum thickness or using gas stripper. At lower terminal voltage, set {3} the Yslits rises even more due to a higher ratio of $\Delta E_q/E$ so it becomes difficult to achieve good transmission of bunched beams, Fig. 2f. The ultimate solution would be to use achromatic systems of bending magnets.

The technique shown in Fig. 3 can be used to measure the energy spread introduced by the buncher or chopper. In Fig. 3 the optimum bunching amplitude ΔE_m is 1.8 kV. This corresponds to a total beam energy spread with charge state minus one of 3.6 keV. According to equation (14), the expected increase of rms diameter of the beam is 0.14 mm. From Fig. 3, the FWHM increased in sound agreement by 0.17 mm.

Time calibration, based on buncher frequency as discussed in Fig. 4 is

a reliable procedure although results in a slightly asymmetric waveform of the pulsed beam. This is probably due to different optics for beams with energy spread. The measured FWHM is quite a high value of a pulse width of 2.3 ns and is consistent with the prediction for minimum time spread $\Delta t_q = 0.84$ ns in Table 1, set {2}, for a Li beam.

5. Conclusions

Beams of $^{1}H^{1+}$, $^{7}Li^{3+}$, $^{16}O^{6+}$ and $^{58}Ni^{12+}$ ions were pulsed successfully. In the case of the tandem accelerator, very short bursts of ions can be produced at low energy by a single gap to which sine wave voltage modulation is applied followed by trimming with choppers at high energy. The measurements carried out to test the performance of the bunching system confirm the validity of the expressions used in the design. Good correlation was obtained between observed bunched pulsed waveforms and theoretically predicted waveforms in a wide range of beam parameters. The transit time and beam size variations due to bunching energy spread, low energy chromatic aberrations and the path in the 90° magnet are an important limitation in performance for light ions. The ideal solution would be to have an isochronous transport for both low energy optics and high energy analyzing systems. For the heavy ions, the performance restrictions are caused by transit time variation due to energy spread in the ion source, stripper foil, path length differences through the Pelletron and the 90° analyzing magnet [35,36]

CRediT authorship contribution statement

Nikolai R. Lobanov: Conceptualization, Methodology, Formal analysis, Writing - original draft. **Peter Linardakis:** Writing - review & editing, Investigation, Validation, Formal analysis. **Daniel Tempra:** . **:** Writing - review & editing, Data curation, Visualization.

Declaration of Competing Interest

The authors declare that they have no known competing financial interests or personal relationships that could have appeared to influence the work reported in this paper.

Acknowledgements

This work has been supported by the Australian Federal Government Superscience/EIF funding and the NCRIS HIA capability. The authors thank their past colleagues from the Department of Nuclear Physics, George Dracoulis and David Weisser, who provided insights and expertise in electrostatic accelerators and commissioned the first prototype of pulsing system at early stage of the project.

References

[1] F.J. Lynch, R.N. Lewis, L.M. Bollinger, W. Henning, O.D. Despe, Beam buncher for heavy ions, Nucl. Instr. Meth. 159 (1979) 245–263.
[2] S.J. Skorka, Design considerations and present status of beam bunching technology, in proceedings of the 3rd International Conference on Electrostatic Accelerator Technology, Oak Ridge, (1981), 130.
[3] R. Repnow, M. Goldschmidt, K. Haberkant, K.D. Hildenbrand, G. Hortig, F. Jaeschke, B. Martin, R. Schule, Nucl. Instrum. And Meth. 122 (1974) 188.
[4] S.I. Tabor, G. Neuschaefer, Experiments with sub-nanoseconds tandem beam pulses, IEEE Trans. On Nucl. Sci., NS-30, N 2 (1983) 1504–1507.
[5] A. Sarkar, S. Ghosh, P. Barua et al, Single-gap multi-harmonic buncher for NSC pelletron, Amer. Inst. of Phys. Conf. Proc. 473 (ed. K. Shepard) (1999) 272-278.
[6] Q. Zhao, V. Andreev, J. Brandon, G. Machicoane, F. Marti, J. Oliva, J. Ottarson and J. Vincent, Design and test of the triple-harmonic buncher for the NSCL re-accelerator, Proceedings of LINAC08 Conference (1908) 948-950.
[7] K. W. Zieher, G. Hochschild, A. Hornung, J. P. Fouan, J. Gastebois and P. Joly, Operation of the Karlsruhe superconducting post accelerator test section in the Saclay tandem heavy ion beam, Proceedings of the 1979 Linear Accelerator Conference, Montauk, New York, USA (1979) 114-117.
[8] G.R. Mitchel, J.E. McGregor, Long life buncher grids for heavy ion particle accelerators, Rev. Sci. Instrum. 61 (12) (1990) 3913–3914.
[9] P.N. Ostroumov, V.N. Aseev, A. Barcikowski, B. Clifft, R. Pardo, S.I. Sharamentov, M. Sengupta, Beam test of a grid-less multi-harmonic buncher, in Proceedings of PAC07, New Mexico, USA, 2007, pp. 2242–2244.
[10] R. L. Poirier, P. Bricault, G. Dutto, K. Fong, R. Laxdal, A.K. Mitra, L. Root.
[11] P. Schmor, G. Stanford, B. Uzat, Y.V. Bylinsky and A. Facco, ISAC rf structures and commissioning, Proceedings of EPAC 2000, Austria (2000) 321-323.
[12] J.H. Anderson, R. Batchelor, F.A. Howe, G. James, J.H. Towle, Klystron bunching of the ion beam of a 5.5 MV Van De Graaf, Nucl. Instrum. And Meth. 41 (1966) 30–40.
[13] I. Ben-Zvi, M. Birk, E. Dafni, J.S. Sokolovski, A chopper-buncher system for the Rehovolt pelletron, Nucl. Instrum. And Meth. 204 (1983) 255–260.
[14] W.T. Milner, G.D. Alton, D.C. Hensley, C.M. Jones, R.F. King, J.D. Larson, C. D. Moak, R.O. Sayer, Transport of DC and Bunched Beams through a 25 MV Folded Tandem Accelerator, IEEE Transactions on Nuclear Science, NS-22 N3 (1975) 1697–1701.
[15] W.T. Milner, Double-Drift Beam Bunching Systems, IEEE Transactions on Nuclear Science, NS-26, N 1 (1979) 1445–1449.
[16] L. Rohrer, H. Jakob, K. Rudolph, S.J. Skorka, The four gap double drift buncher at Munich, Nucl. Inst. and Meth. In Phys. Res. 220 (1984) 161–164.
[17] J. W. Noe, Operation of the upgraded Stony Brook FN tandem, in proceedings of the 3rd International Conference on Electrostatic Accelerator Technology, Oak Ridge, (1981), 55-58.
[18] E.A. Wadlinger, Buncher system parameter optimization, IEEE Trans. On Nucl. Sci., Vol. NS-28, N 3 (1981) 2630–2632.
[19] A. Facco, F. Scarpa, V. Zvviagintsev, Status of the non-rfq resonators of the PIAVE heavy ion linac, Proceedings of EPAC 2000 (2000) 2037–2039.
[20] J.Z. Jiang, X.H. Zhou, Q. Wang, F. Wang, W.M. Jiang, Buncher in the beam line from ECR to SFC, Proceedings of 13th International Conference on Cyclotrons and their Applications, Canada, Vancouver, 1992, pp. 618–620.
[21] K. Fong, M. Laverty, S. Fang, W. Uzat, Sawtooth Wave Generation for Pre- Buncher Cavity in ISAC, Proceedings of 17th Particle Accelerator Conference, Canada, Vancouver, 1997, pp. 3057–3059.
[22] R.C. Rogers, Design of a beam buncher using a half-cosine driving function, Proceedings of 13th International Conference on Cyclotrons and their Applications, Canada, Vancouver, 1992, pp. 629–633.
[23] J.Y. Tang, J.Z. Jiang, A.M. Shi, Z.K. Yin, Y.F. Wang, Linear bunchers and half-frequency bunching method, Nucl. Instrum. And Meth, Phys. Res. A 455 (2000) 533–538.
[24] A. Chabert, Ch. Ricard, L. Boy, B. Monsanglant and W.Le. Coz, The linear buncher of SPIRAL. Beam test of a prototype, Nucl. Instrum. And Meth. In Phys. Res. A 423 (1999) 7-15.
[25] M. Olsmats, B. Wannberg, Calculations on the ion-beam transport system of the tandem accelerator at Uppsala, Nucl. Instrum. And Meth. 107 (1973) 563–568.
[26] G.A. Norton and G.M. Klody, MeV Ion Implantation Systems for Production Processing of Silicon Wafers, IEEE Trans. Nucl. Sci., NS-30, (1983), 1701-1704.
[27] P. Linardakis, D. Tempra, N.R. Lobanov, Nanosecond pulsing for tandem accelerator, in proceedings of the International Particle Accelerator Conference IPAC19, Melbourne, Australia (2019) 1673–1675, https://doi.org/10.18429/JACoW-IPAC2019-TUPRB001.
[28] J.H. Anderson, D. Swann, A bunching and chopping system for the generation of short duration ion bursts, Nucl. Instrum. And Meth. 30 (1964) 1–22.
[29] G. Doucas, Energy distribution of negative ions sputtered from caesiated surfaces, Int. Journal of Mass Spectrom. Ion. Phys. 25 (1977) 71–87.
[30] J.H. Billen, Emittance calculations and measurements for a sputter-type negative-ion source, Nucl. Instrum. And Meth. In Phys. Res. 220 (1984) 225–250.
[31] J.D. Larson, Beam transport through electrostatic accelerators and matching into post accelerators, Nucl. Instrum. And Meth, Phys. Res. A 244 (1986) 192–200.
[32] G.D. Alton, J.W. McConnell, The emittances and brightnesses of high intensity negative ion sources, Nucl. Instrum. And Meth, Phys. Res. A 268 (1988) 445–455.
[33] J.D. Lawson, The physics of charged-particle beams. Oxford, New York: Clarendon Press 1977.
[34] N. R. Lobanov, P. Linardakis and D. Tsifakis, Tuning the superconducting linac at low beam intensities, in Proc. 17th International Conference on RF Superconductivity, Whistler, BC, Canada, 2015, pp. 602-606.
[35] N.R. Lobanov, T. Tunningley, P. Linardakis, Improved transmission of electrostatic accelerator in a wide range of terminal voltages by controlling the focal strength of entrance acceleration tube, Nuclear Inst. and Methods in Physics Research B 421 (2018) 38–44.
[36] D. Tsifakis, N.R. Lobanov and P. Linardakis, Development of a beam pulse monitor for the heavy ion accelerator facility, in proceedings of the International Beam Instrumentation Conference IBIC 2015, Melbourne, Australia, (2015), 27-29.